An Experimental and CFD Analysis of a Two-Phase Flow Air Induction Nozzle with Agricultural Application

Foad Vashahi[1], Sothea Ra[1], Yong Choi[2] and Jeekeun Lee[3]
[1]*Mechanical System Engineering, Chonbuk National University, 54896, Jeonju-si, Jeollabuk-do, Korea, Republic of*
[2]*Agricultural Engineering, Rural Development Administration, Farming Automation Division, 560-500310 Nongsaengmyeong-ro, Wansan-gu, Jeonju-si, Jeollabuk-do, Korea, Republic of*
[3]*Division of Mechanical System Engineering, Chonbuk National University, 54896, Jeonju-si, Jeollabuk-do, Korea, Republic of*

Keywords: CFD, VOF Model, Two-Phase Flow, Air Induction Nozzle (AIN), Drift Reduction.

Abstract: The two phase flow parametric study on the air induction nozzle is presented with water and air as working fluid where liquid was supplied at the pre-orifice with various inlet pressures ranged from 3 to 6 bar. The interaction between air and water at molecular level at the orifice exit leads to forming a strong shear layer intensified with increase in inlet pressure. Mean diameter and void fraction in each bubble and their individual shapes is adjusted prior to the desired criteria. Thus, it is vital to regulate the ratio of intake air to the supplied liquid so that the generated micro bubbles fit the design criteria. CFD analysis was accompanied via commercial software STAR CCM+ from cd-adapco and validated against experimental data to find the most appropriate turbulence model. Then, the chosen model is used to investigate design parameters and their effect on the desired parameters. A volume of fluid (VOF) method of RANS models used to undertake the air-water interaction. Results of such comparison revealed minor priority of the Realizable k-ε to the k-ω model. In addition, the unsteady state solution presented remarkable predictions in compare to that of steady state solution in particular predicting air behaviour.

1 INTRODUCTION

Spray drift is becoming significantly important aspect of every spray operation. With greater diversification of crops, higher active or non-selective herbicides, and greater awareness of pesticides effects on the environment, spray drift management has been widespread. Nozzles can play an important role in drift management due to the ability to provide a wide range of droplet sizes which determines how effective the spray deposit is, and how much the spray itself will drift (Wolf and Kutcher, 2001). Furthermore, their structure is relatively simple and low cost.

Air-induction/venturi nozzle systems appeared to be very promising for improving efficiency and drift reduction, in particular, for the systemic herbicides usage. Large droplets generated by these nozzles, results in a reduction in the surface coverage area which is implementable in insecticides and fungicides (Miller et al., 2003 and Tobi et al., 2008). These nozzles are relatively new; therefor the mechanism of droplet generation and mixing process is not fully understood.

The design characteristics of the spray under the influence of the venturi throat diameter and final orifice size was investigated (Butler Ellis et al., 2002). It was shown that increasing both factors resulted in a rise in airflow rate, as did a reduction in liquid flow rate. In addition, droplet size was found affected mostly by the size of the final orifice and slightly by the air intake. The amount of air sucked into the nozzle was found highly dependent on the chemical mixture being sprayed and the nozzle design (Dorr et al., 2013). Also, the air inclusion was found crucial for modifying the droplet behaviour and their impact on target surface and the ability of spray droplets to retain air bubbles will be a function of spray liquid properties (Miller et al., 2000). The air induction design is more sensitive to changes in physical characteristics of the spray liquid than conventional hydraulic pressure nozzles.

Vashahi, F., Ra, S., Choi, Y. and Lee, J.
An Experimental and CFD Analysis of a Two-Phase Flow Air Induction Nozzle with Agricultural Application.
DOI: 10.5220/0005960601720178
In *Proceedings of the 6th International Conference on Simulation and Modeling Methodologies, Technologies and Applications (SIMULTECH 2016)*, pages 172-178
ISBN: 978-989-758-199-1

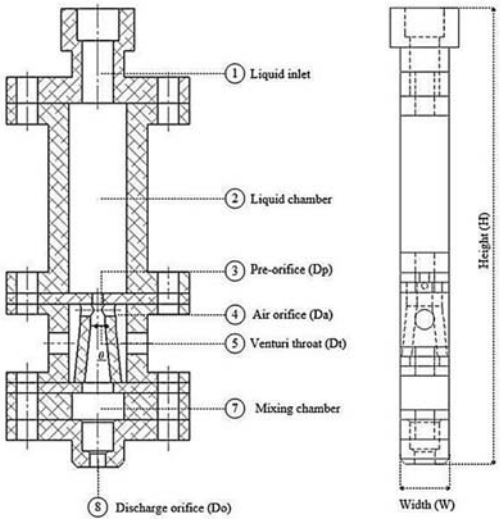

Figure 1: Schematic of the 2D Air Induction Nozzle (AIN).

The amount of air intake into the nozzle plays an important role on the air induction nozzle characteristic. For sure, more research is needed to verify the effect of several geometrical parameters, especially strength of each parameter on the spray characteristic of the nozzle.

Computational Fluid Dynamic (CFD) has found its way through design process of AIN. A mixture model of algebraic slip model along with standard k-ε turbulent model was applied on coaxial flows (Yadav et al., 2008). This approach required solving a slip velocity equation along with momentum and continuity equations for ejector between gas and liquid. Applying standard k-ε turbulent model for gas-liquid ejector was confirmed by other scientists such as (Kandakure et al., 2005 and Li et al., 2012).

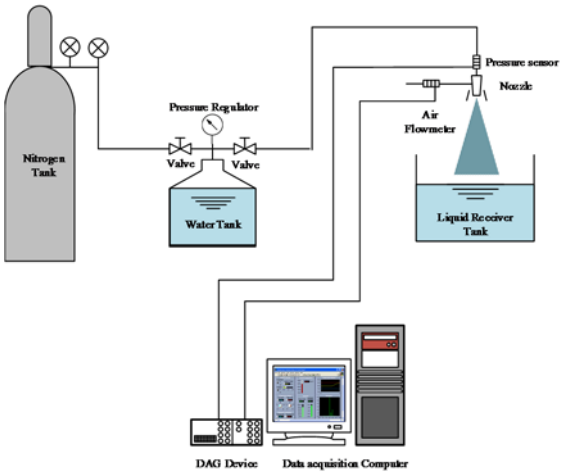

Figure 2: Experimental apparatus for the 2D AIN.

It was concluded that the standard k-ε model is applicable to model the turbulent behaviour of flow in ejector due to its robustness and reasonable accuracy. They found that the Standard k-ε model predicts the entrainment performance satisfactorily for gas-liquid ejectors. Meanwhile the entrained mass flow rates calculated by the SST k-ω model and the Standard k-ε model showed deviation from the experimental results (Zhu et al., 2009).

In this paper, a comparison of CFD with experimental results on a 2D AIN is established to find the proper turbulence scheme and then based on the validate results a 3D nozzle is developed. The strength of design parameters on the ALR reduction is investigated and a theoretical design is proposed.

2 EXPERIMENTAL APPARATUS

The air induction nozzle is composed of several parts such as: liquid chamber, pre-orifice, venturi with air orifice, mixing chamber and discharge orifice as demonstrated in Figure 1. Detailed dimensions are given in Table 1. Front and back view of the nozzle were covered by two transparent acrylic plates which are assembled by bolts and nuts. Plastic seals were used to prevent fluid leak-out from the nozzle body. The main facilities components for this experimental set up are shown in Figure 2. Liquid (water) is injected to the nozzle from the pressurized tank. Two ball valves are located on the top of pressurized water tank and are used to control the pressure and water flowrate. The liquid injection pressure of 3 to 6 bar was read at the liquid inlet port through various experimental conditions. Liquid receiver is set up at the bottom of the nozzle and the liquid mass flowrate is measured from the discharge orifice of nozzle.

Table 1: Detailed description of the 2D AIN.

Part name			Units
Height of nozzle	H	93.0	mm
Width of nozzle	W	10.0	mm
Pre-orifice diameter	Dp	ϕ 2	mm
Throat diameter	Dt	ϕ 3.2	mm
Divergent angle	θ	6.0	°
Air orifice diameter	Da (equi.)	ϕ 3.8	mm
Discharge orifice	Do	ϕ 4.2	mm

The principle of air induction nozzle suggests that within the venturi throat section a vacuum pressure is created and air is drawn into the nozzle through air orifice side. Thus, mixing with the spray liquid stream as it passes by while liquid flows from liquid

chamber through the pre-orifice. As the result air-filled droplets are created. Therefore, system was not equipped with any air supply tank and air orifice is opened to the atmospheric with the room temperature condition of 20°C. It is anticipated that the amount of air flowrate should change according to the changing of pressure supply. A NI-LabVIEW based data acquisition system is used to store all data from measurement sensor devices. The pressure sensor (ETM-375-500A) is located before the nozzle inlet. In addition, in order to measure the entrainment of air, the gas mass flow sensor FS4008-50 with a pressure drop of approximately 600Pa is required to be placed right before the air orifice. This amount of pressure drop is adequately low so that the measurement is considered highly accurate.

3 NUMERICAL SCHEME AND BOUNDARY CONDITION

The analysis was based on the commercial CFD software STAR CCM+ Version 10.06.010, which applies the finite volume method. Steady and implicit unsteady segregated flow solvers were compared implementing a second-order scheme for temporal discretization. Volume of Fluid (VOF) method was used to simulate the interaction of a two phase flow within the nozzle. The VOF model describes the fluid phase in the volume with the assumption of shared velocity, pressure and temperature fields. Here the iso-thermal solver was used thus the temperature effects are not considered. The conservation equation that describes the transport of volume fractions α_i is given :

$$\frac{d}{dt}\int_V \alpha_i dV + \int_S \alpha_i (v - v_g) da = \int_V \left(S_{\alpha_i} - \frac{\alpha_i}{\rho_i}\frac{D\rho_i}{Dt} \right)_i dV$$

Where, $\alpha_i = V_i/V$ is the volume fraction, S_{α_i} and $\frac{D\rho_i}{Dt}$ are the source or sink of the i^{th} phase and the material or Lagrangian derivative of the phase densities ρ_i, respectively (cd-adapco, 1987).

The Reynolds averaged Navier stocks (RANS) approach is used validating against experimental data. Substituting the Reynolds decomposition into the Navier-Stokes equations yields the general equations, which are termed the mean-momentum or Reynolds equations. The *k-ε* and *k-ω* models are generally classified into the two-equation models where each is frequently used as solutions to the RANS equations (Pope, 2000). The *Realizable k-ε* model (RKEM) satisfies certain mathematical constrains for the normal stress that are consistent with the physics of turbulent flows. In this study, it is accompanied by a two-layer near-wall-treatment formulation because the traditional k-ε approach is not capable of resolving the viscous forces in the viscous sub-layer.

Air enters from two sides of the nozzle with inlet boundary condition of zero gauge pressure and liquid water enters from the top of the nozzle with a mass flow corroborating to the experimentally applied pressure. Air and water were treated as constant density at 21 and 20°C respectively. No-slip boundary conditions and an all y+ treatment were applied to obtain velocity profiles in wall-affected regions. $Y^+<5$ was achieved by adjusting 8 prism layers near the walls along by applying all y^+ treatment.

The polyhedral mesh was generated from a maximum of 0.4 mm down to 0.004 mm within the area where high shear layer is anticipated due to the interaction of air and water. The total cell count varied from 5.0 to 8.0×10^5 depending on the geometrical study. Unsteady simulations were performed via marching time of 5×10^{-5} s within inner iterations of 5 to achieve a courant number<1.

4 RESULTS AND DISCUSSION

4.1 Turbulence Model Validation

Figure 3 presents a comparison between inlet pressure achieved experimentally and the calculated one from the CFD code (The error percentage is given as $[(V_{Exp.}-V_{CFD})/V_{Exp}] \times100$). A slight overestimation for the equivalent mass flow rate at inlet was given by the k-ω model (Menter, 1994). Due to better performance of the k-ε model, the unsteady case was limited to this model and not performed for the k-ω one. Steady and unsteady k-ε results resembled and both well predicted the inlet pressure. However, unsteady simulation was found to be superior to other models. It is vital to note that in terms of simulation time, the steady ones are preferred. On the other hand, if case is care about accuracy then the unsteady simulation is the sophisticated choice and fast solutions should be sacrificed. Add to this, the comparison of the air-liquid-ratio (ALR) acquired from the experiment and CFD given in Figure 4, indicates absolute superiority of unsteady simulations to that of steady in both cases of k-ε and k-ω.

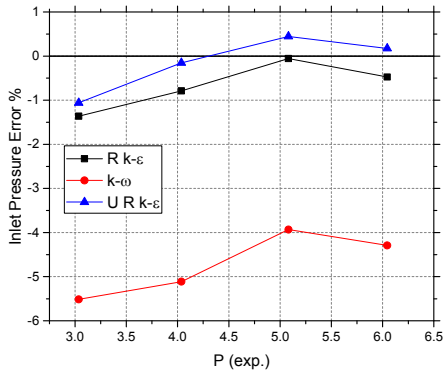

Figure 3: Error percentage of CFD against experimental data.

This shows the unsteady nature of these flows and denies the application of steady state solutions to these cases. Also shows that the VOF method is applicable to predict the intake air amount and the ratio of air to water flow. Revealing the unsteady solver to the steady one, the effect of throat diameter (D_t) on the air suction is investigated experimentally and numerically.

Figure 5, shows two important points. First, increasing the throat diameter at different inlet pressures would result in a linear rise in the amount of air entrained. The reason this is happening is that increase in throat diameter, simply provide a wider passage for the entrained flow and less kinetic energy is required to overcome the liquid flow exited from the liquid orifice. These effects are more pronounced varying from certain range of diameter and become less significant once that certain diameter is exceeded due to the air excess within the mixing chamber.

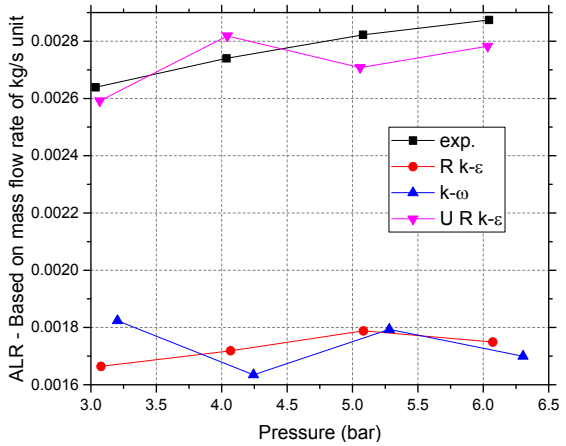

Figure 4: Comparison of the ALR of different turbulence model for inlet pressures of 3.0, 4.0, 5.0 and 6.0.

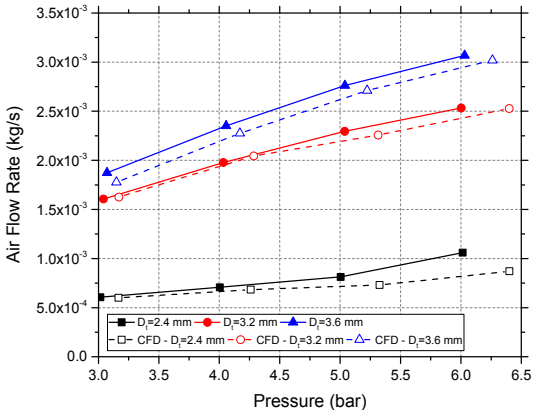

Figure 5: Effect of throat diameter (D_t) on the air entrainment.

Secondly, although some over and under estimations are given, the unsteady simulation results were found to be in agreement with the experimental results both qualitatively and quantitatively and provide a prediction capability where no experimental result is available.

4.2 Parametric Study on the Theoretical 3D AIN

Since the reliability of the turbulence model with a certain degree of estimation error was found acceptable, parametric studies on the 3D AIN were then performed via CFD as the next step after the model validation. To this extent, a base model was designed with an assumption of D_p remains constant and then different parameters were modified to achieve the target ALR<0.00025. A schematic of a the air/water interaction section from pre-orifice down to a distance through the divergence section is given in Figure 6a, to get familiar with the upcoming introduced geometrical parameters such as D_p. Constructed polyhedral mesh given in Figure 6b. varies at the range of 600,000 cells for different cases and the same methodology as the 2D AIN was applied for y^+, turbulence model and other solver settings.

Two case of D_a=0.2 and 1.0 mm was compared to the base simulation case of D_a=0.5. Figure 7 shows the effect of decreasing D_a on the air intake at inlet constant pressure of 3 bar. It is seen that a fall in D_a leads to a decrease in the ALR down to 0.0008 which is still higher than the target value. The effect of the throat diameter on the air intake is marked with the red line in Figure 7. Same tendency as the 2D AIN can be seen where the increase in the throat diameter leads to an increase in the ALR.

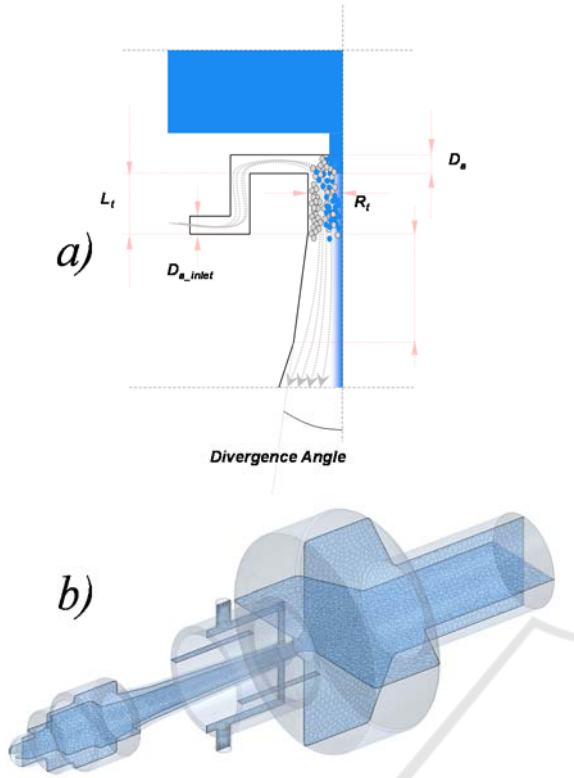

Figure 6: a) Schematic of the interaction area where liquid meets the entrained air and the geometrical parameters – b) Polyhedral mesh generation on the 3D AIN concept.

Although the reduction trend of ALR with a decrease of D_a occurs with a steeper slope, the decrement of D_t down to a minimum diameter of 0.55mm resulted in a slightly lower ALR. Thus, it can be seen that within roughly the same ratio to D_p the increase or decreasing amount of air intake resemble in both cases where the strength is weighted to the D_t side.

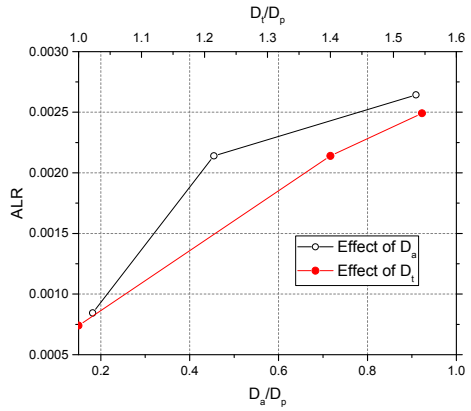

Figure 7: Effect of Da and Dt on the (ALR).

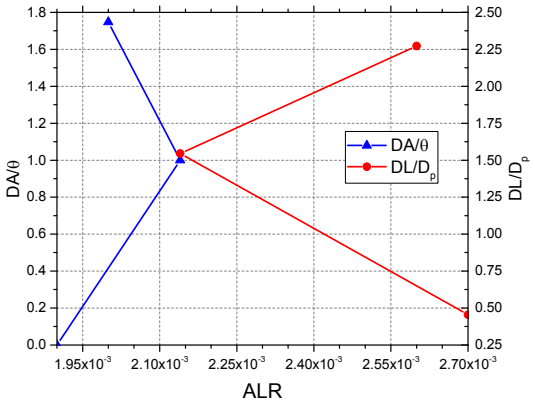

Figure 8: Effect of Divergence angel and divergence length on the ALR.

The effect of Divergent Angle and length is given in Figure 8. Parameters were normalized by the base angle and D_p respectively. Zero divergent angle dictates a state where the mixing chamber is straight and it is sloped as the angle ratio is increases. It can be seen that the ALR first increases then decreases. Yet these changes are insignificant in compare to D_a and D_t effects on the air/liquid ratio. At the same time decrease and increase of divergent length results shows contradictory behaviour to that of divergent angle where minimum is located at the central DL/D_p at midpoint. This shows that the mixing chamber and mixing length section are of minor importance in terms of reducing the ALR.
Study of the reduction air inlet area and how it affects the ALR is demonstrated in Figure 9. In general, it shows that any increase in the total area results in a decrease in the air suction rate.

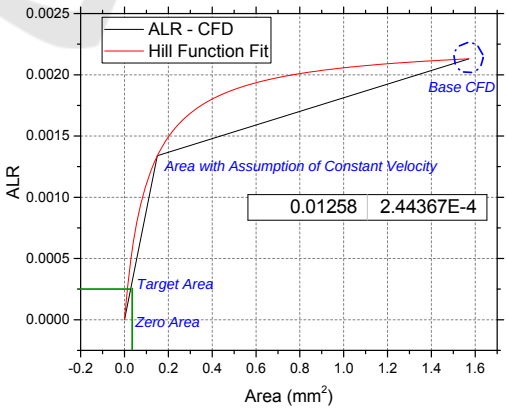

Figure 9: Effect of air inlet total area (A1+A2).

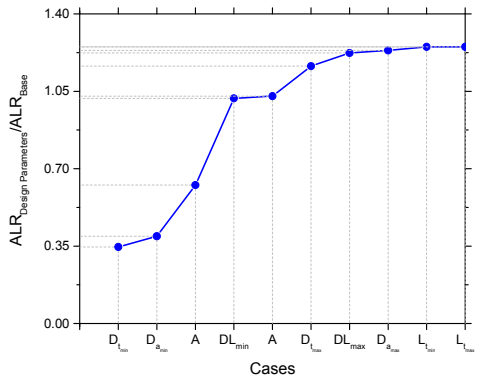

Figure 10: ALR comparison of various study cases – ALR is normalized to the base CFD results.

Rough estimation of air inlet area with an assumption of velocity constant gave a 0.18 mm^2 total area for air inlet on bases of simple continuity equation. Simulation of this predicted area gave an ALR of 0.0013 indicating the deficiency of the first assumption. Thus the estimation was enhanced by the fitted hill function curve to get an appropriate estimation of the required inlet area. The fitted curve demonstrates that in order to achieve the target ALR, the total area on both inlets should be decreased down to a maximum of 0.012 mm^2. This cannot be considered a practical value since it is too small to manufacture. Different air inlet areas were simulated and added to the simulation table. But in order to have a clear look on the parameters and their effects on the ALR a simple figure is required.

To this extent, a summary of the given study is presented in Figure 10 where all the parameters and their effects on ALR are compared. It can be seen that the major impact on the ALR are of "D_t, D_a, and A" parameters, respectively while the throat length from varying from minimum, down to air orifice to its maximum value, has the worst impact on the ALR by increasing it. However, simulating all these cases, the ALR did not reach the desired value of 0.00025. Thus, all the geometrical parameters together should be considered in order to reduce the ALR to the desired target. A more scrutiny shows that although D_t has decreased ALR down to the minimum in relevance to all the other parameters, yet the ALR difference for the D_a was higher. This indicates that the strength of these two parameters can be considered higher than the rest in order.

A combination of optimized design parameters of D_t/D_p=1.09, D_a/D_p=0.18, and A=0.019 mm^2 altogether gave an ALR of 0.000236 which is reasonably decreased and falls within the desired range. It should be noted that the effect of D_p should also be considered along with other design criteria otherwise other dimensions may suggest unrealistic values.

5 CONCLUSIONS

An experiment on the 2D Air Induction Nozzle (AIN) was developed and compared to the simulation results of steady and unsteady k-ω and k-ε as the first step to design a three dimensional AIN with agricultural application. It was shown that the unsteady model superiorly gives better results due to the nature of flow, in particular, predicting the Air Liquid Ratio (ALR). Then, the theoretical three dimensional model was developed and strength of each parameters such as D_t,D_a, air inlet area, L_t, DA and DL was studied while keeping the D_p constant. It was found that the D_t and D_a have the highest impact on the ALR where the throat length has the least effect in decreasing ALR. An optimized 3D model was then simulated and an ALR of 0.000236 achieved.

ACKNOWLEDGEMENTS

This work was carried out with the support of "cooperative Research Program for Agricultural Science & Technology Development (Project No. PJ011719)" Rural Development Administration, Republic of Korea.

REFRENCES

Wolf, T. M., Kutcher, H. R., March 2001. *Spray application methods to maximize sclerotinia control in Cansada with foliar fungicide,* Canola Agronomic Research Program (CARP AG#98-23), final report.

Miller, P. C. H., Powell, E. S., Orson, J. H., Kudsk, P., and Mathiassen S., September 2003. *Defining the size of target for air induction nozzles,* The Home-Grown Cereal Authority (HGCA), project report 317.

Tobi, I., Saglam, R., Turgut, M. M., October 2008. *Equipment and application techniques reduced agricultural pesticide drift, 10th International Congress on Mechanization and Energy in Agriculture* Antalya-TURKIYE.

Butler Ellis, M. C., Swan, T., Miller, P. C. H., Waddelow, S., bradly, A., Tuck, C.R., 2002. *Design Factors affecting spray characteristics and drift performance of Air induction nozzles.* Biosystems Engineering 82(3), 289-296.

Dorr, G. J., Hewitt, A. J., Adkins, S. W., Hanan, J., Zhang, H., Noller, B., 2013. *A comparison of initial spray characteristics produced by agricultural nozzles.* Crop Protection 53 (2013) 109-117.

Miller, P. C. H., Butler Ellis, M. C., 2000. *Effects of formulation on spray nozzle performance for applications from ground-based boom sprayers.* Crop Protection 19 (2000) 609-615.

Yadav, R. L, Patwardhan, A. W., 2008. *Design aspects of ejectors: Effects of suction chamber geometry.* Chemical Engineering Science 63 (2008) 3886 – 3897.

Kandakure, M. T., Gaikar, V. G., Patwardhan, A. W., 2005. *Hydrodynamic aspects of ejectors.* Chemical Engineering Science 60 (2005) 6391-6402.

Li, C., Li Y., Wang L., 2012. *Configuration dependence and optimization of the entrainment performance for gas-gas and gas-liquid ejectors.* Applied Thermal Engineering 48 (2012) 237-248.

Zhu, Y., Cai, W., Wen, C., Li, Y., 2009. *Numerical investigation of geometry parameters for design of high performance ejectors.* Applied Thermal Engineering 29 (2009) 898–905.

Pope, S.B., 2000. *Turbulent Flows*, Cambridge University Press.

Menter, F. R., 1994. *Two-equation eddy-viscosity turbulence models for engineering applications.* AIAA Journal, Vol. 32, No. 8 (1994), pp. 1598-1605.

Cd-adapco, 1987. *STAR-CCM+ manual,* Version 10.06.010.